RSC Advances

PAPER

View Article Online
View Journal | View Issue

Cite this: *RSC Adv.*, 2022, **12**, 11190

Revealing the different performance of Li_4SiO_4 and Ca_2SiO_4 for CO_2 adsorption by density functional theory†

Wenjing Yu,[a] Qian Xu,*[a] Shenggang Li,*[b] Xiaolu Xiong,[a] Hongwei Cheng,[a] Xingli Zou[a] and Xionggang Lu[a]

Received 16th February 2022
Accepted 4th April 2022

DOI: 10.1039/d2ra01021f

rsc.li/rsc-advances

To reveal the difference between Li_4SiO_4 and Ca_2SiO_4 in CO_2 adsorption performance, the CO_2 adsorption on Li_4SiO_4 (010) and Ca_2SiO_4 (100) surfaces was investigated using density functional theory (DFT) calculations. The results indicate that the bent configuration of the adsorbed CO_2 molecule parallel to the surface is the most thermodynamically favorable for both Li_4SiO_4 and Ca_2SiO_4 surfaces. The Li_4SiO_4 (010) surface has greater CO_2 adsorption energy ($E_{ads} = -2.97$ eV) than the Ca_2SiO_4 (100) surface ($E_{ads} = -0.31$ eV). A stronger covalent bond between the C atom of adsorbed CO_2 and an O_S atom on the Li_4SiO_4 (010) surface is formed, accompanied by more charge transfer from the surface to CO_2. Moreover, the Mulliken charge of O_S atoms on the Li_4SiO_4 (010) surface is more negative, and its p-band center is closer to the E_f, indicating O_S atoms on Li_4SiO_4 (010) are more active and prone to suffering electrophilic attack compared with the Ca_2SiO_4 (100) surface.

1. Introduction

CO_2 capture, storage and utilization (CCSU) is considered as one of the most promising technologies for reducing anthropogenic CO_2 emission, which can lead to global warming. Solid inorganic sorbents have been proven to efficiently remove CO_2 at high temperatures, and are more economical and effective than low-temperature amine-based materials in CO_2 capture from high temperature exhaust gas.[1] Lithium orthosilicate (Li_4SiO_4) is one of the best CO_2 capture sorbents due to its significant advantages, such as large adsorption capacity, low regeneration temperature, and good adsorption and desorption cycle stability.[2–4] There have been a lot of experimental studies on Li_4SiO_4 as an adsorbent to capture CO_2, including the synthesis method,[5,6] kinetic behavior[7–9] and modification of Li_4SiO_4.[10–12] However, lithium is relatively expensive and not very abundant in the earth's crust. In particular, lithium batteries have been widely used as a source of power or energy for a lot of things from portable electronics to electric vehicles. As a result, the demand for lithium is increased which leads directly to an increase of its price. Accordingly, it is very difficult to apply lithium-based ceramics on a huge scale to capture CO_2 economically and sustainably. Meanwhile there are abundant resources basic silicates all over the world, especially calcium silicates (Ca_2SiO_4) are often found in the industrial by-products named as slags generated during iron and steel production. Furthermore, Ca_2SiO_4, similar to Li_4SiO_4, is thermodynamically favorable for CO_2 capture from room temperature to 572 °C at ambient pressure, and Gibbs free energy changes for the carbonation of Ca_2SiO_4 and Li_4SiO_4 were calculated by HSC Chemistry 6.0 and shown in Fig. 1. However, the slow diffusion and reaction of carbonation between CO_2 and calcium silicates is a common issue even at high temperatures in the case of no participation of water.[13] It was found that the amount of CO_2 captured with Ca_2SiO_4 is little at the temperature range from room temperature to 572 °C in our previous study. Zhao *et al.*[14,15] applied Ca_2SiO_4 as the inert material to enhance the sintering resistance and cyclic stability of CaO during multiple sorption/desorption of CO_2. It could be deduced that Ca_2SiO_4 is much inerter for carbonation compared with Li_4SiO_4 at the high temperatures.

The investigation on the effect of the electronic structure of the silicates on their carbonation reactivity should be very important for understanding deeply the different carbonation behaviors for Li_4SiO_4 and Ca_2SiO_4, and developing new approaches to improve the carbonation activity of silicates.

There are some investigations about CO_2 adsorption on the surface of the oxides and silicates with the first-principles calculations. Kim *et al.*[16] made an assessment of Li_2O and Na_2O surfaces for CO_2 adsorption based on DFT calculations. They found that the introduction of dopant atoms larger than host metal atoms of the surfaces can negatively increase CO_2 adsorption energies. Kumar *et al.*[17] studied the CO_2 adsorption on different terminations of Cr_2O_3 surfaces with DFT calculations and found that carboxylate species are formed on O layer

[a]Shanghai University, China
[b]Shanghai Advanced Research Institute, China

† Electronic supplementary information (ESI) available. See https://doi.org/10.1039/d2ra01021f

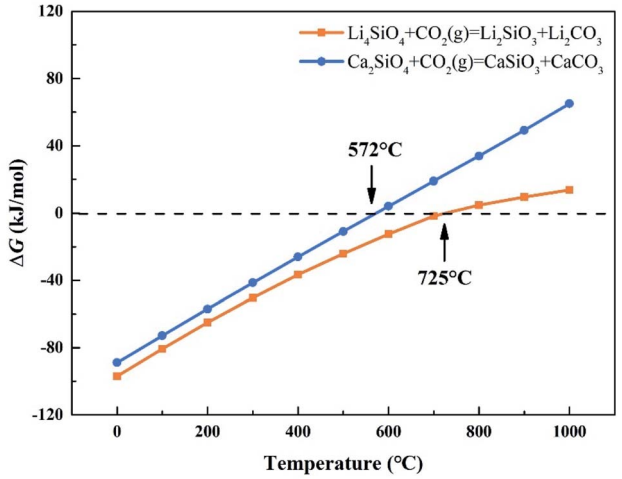

Fig. 1 Relationship between ΔG and temperature of carbonation reaction between CO_2 and Li_4SiO_4 and Ca_2SiO_4.

terminated-(0001), and carbonate species are formed on O layer terminated-(10$\bar{1}$2) and Cr layer terminated-(01$\bar{1}$2), indicating that the formation of physisorbed and chemisorbed species depends on different surface terminations. Kang *et al.*[18] thermodynamically evaluated the CO_2 capture potential of Mg_2MO_4 (M = Si, V, and Ge). Their results indicated that the critical temperature at which CO_2 can be absorbed, increased with decreasing Pauling electronegativity of the M site.

There are several investigations for Li_4SiO_4 on its structural, electronic, lattice dynamical and thermodynamic properties. Duan[19] and Tang *et al.*[20] found the covalency properties of Li_4SiO_4 mainly resulting from the overlap of O 2p and Si 3p orbitals. Kong *et al.*[21] studied the adsorption mechanism of H_2O on the Li_4SiO_4 (010) surface. It was suggested an interaction between adsorbed H_2O and Li_4SiO_4 (010) surface, including an electrophilic interaction of hydrogen atom in water with oxygen atoms on the surface and a nucleophilic interaction of oxygen atoms in water with Li atoms on the surface.

Ca_2SiO_4, as the industrial cement clinkers, has been investigated by DFT calculations extensively, and many studies focused on the hydration of Ca_2SiO_4 phases. Qi *et al.*[22] investigated H_2O adsorption on low-index surfaces of Ca_2SiO_4, indicating that electron are mainly transferred from surface atoms to H_2O molecule. Wang *et al.*[23] evaluated H_2O adsorption on β-Ca_2SiO_4 surfaces and found a dual interaction between H_2O and β-Ca_2SiO_4 (100) surface. Wang *et al.*[24] also studied the relationship between reactivity and electronic structure of α'_L-, β- and γ-Ca_2SiO_4 for hydration process. They found that the higher hydration reactivity of α'_L- and β-Ca_2SiO_4 compared with γ-Ca_2SiO_4 are attributed to the higher charge density and larger local state density of the active oxygen atoms in α'_L- and β-Ca_2SiO_4. However, there are few investigations about explanation of the different behaviors of carbonation of Ca_2SiO_4 and Li_4SiO_4 on the base of their structural and electronic properties.

Herein, we have systematically investigated the structural and electronic properties of Li_4SiO_4 and Ca_2SiO_4, and the adsorption of CO_2 on the most stable surfaces of Li_4SiO_4 and Ca_2SiO_4 on the base of density functional theory calculations. We tried to reveal the relationship between the electronic structures of Li_4SiO_4 and Ca_2SiO_4 and their reactivity for CO_2 adsorption on the molecular scale. The results of this investigation could converge to a proposed mechanism of CO_2 capture with the orthosilicates, on which the more reactive silicates for CO_2 capture can be screened out as the candidates for CO_2 capture.

2. Computational details

The calculations were performed based on density functional theory (DFT), using Cambridge Series Total Energy Package (CASTEP) code.[25] The exchange-correlation potential was approximated within the generalized gradient approximation

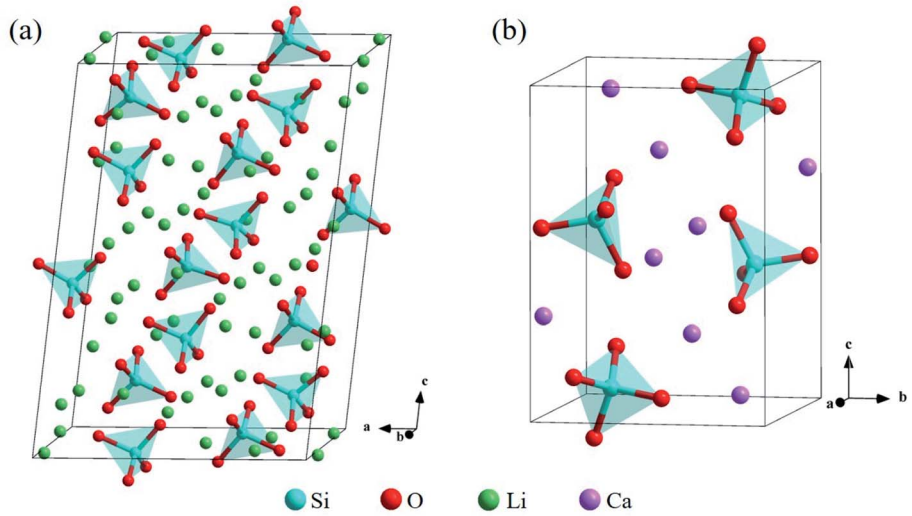

Fig. 2 Crystal structures of (a) Li_4SiO_4 and (b) Ca_2SiO_4. The Si, O, Li and Ca atoms are shown by blue, red, green and purple spheres, respectively.

Table 1 Comparison of calculated lattice constants of Li_4SiO_4 and Ca_2SiO_4 with experimental lattice constants

	Li_4SiO_4			Ca_2SiO_4		
	Cal	Expt[19]	Δ (%)	Cal	Expt[40]	Δ (%)
a (Å)	11.511	11.532	0.18	5.571	5.502	1.25
b (Å)	6.080	6.075	0.08	6.800	6.745	0.82
c (Å)	16.708	16.678	0.18	9.354	9.297	0.61
β (°)	99.15	99.04	0.11	94.295	94.590	0.31

(GGA)[26] using the Perdew–Burke–Ernzerhof (PBE) functional.[27] Dispersion-corrected calculations[28] were performed with Grimme's DFT-D3 methodology.[29] To model Li_4SiO_4 and Ca_2SiO_4, the unit cell ($1 \times 1 \times 1$) was applied for the calculation.

In order to optimize the crystal structures, the plane wave truncation energy and k-points were tested. A cutoff-energy of 650 eV was used for plane wave expansions. The k-points meshes within Monkhorst-Pack[30] framework were set as $3 \times 6 \times 2$ and $4 \times 3 \times 2$ for Li_4SiO_4 and Ca_2SiO_4 respectively. The Broyden–Fletcher–Goldfarb–Shenno (BFGS)[31] minimization algorithm was used to optimize the primitive unit cell. The surfaces of Li_4SiO_4 and Ca_2SiO_4 were cleaved from the optimized bulk structure. All surfaces were kept stoichiometric and neutral to avoid the polarizing electric field. The thicknesses of vacuum layer were set as 15 Å to avoid the interaction between slabs. The convergence criteria were fixed, specifically: the energy change within 1×10^{-5} eV per atom, the force on the atoms within 0.03 eV $Å^{-1}$, the stress on the atoms within 0.05 GPa, and the displacement of atoms within 1×10^{-3} Å. All the initial crystal structures and date were obtained from the Inorganic Crystal Structure Database (ICSD).[32]

3. Results and discussion

3.1. Structural and electronic properties of bulks

The bulk structure of Li_4SiO_4 with the monoclinic phase, which space group is $P21/m$ (no. 11),[33–35] was optimized. The unit cell of Li_4SiO_4 contains 126 atoms, including 14 $[SiO_4]^{4-}$ tetrahedra and 56 Li atoms, as shown in Fig. 2a, which are centrally symmetrical. Meanwhile, the bulk structure of Ca_2SiO_4 with the monoclinic phase, which space group is $P21/n$ (no. 14),[36–38] was optimized as well. The unit cell of Ca_2SiO_4 consists of 28 atoms, including 4 $[SiO_4]^{4-}$ tetrahedra and 8 Ca atoms, as shown in Fig. 2b. The calculated and experimentally measured lattice parameters of Li_4SiO_4 and Ca_2SiO_4 are presented in Table 1, and they are in good agreement, implying the simulation settings are reliable and give reasonable results.

Fig. 3 shows the total density of states (TDOS) and partial density of states (PDOS) for Li_4SiO_4 and Ca_2SiO_4. Electrons occupying the orbitals below and near the Fermi level (E_f) is of great significance to the activity of the crystal materials for chemical reactions,[39] so we focused on the electrons on the

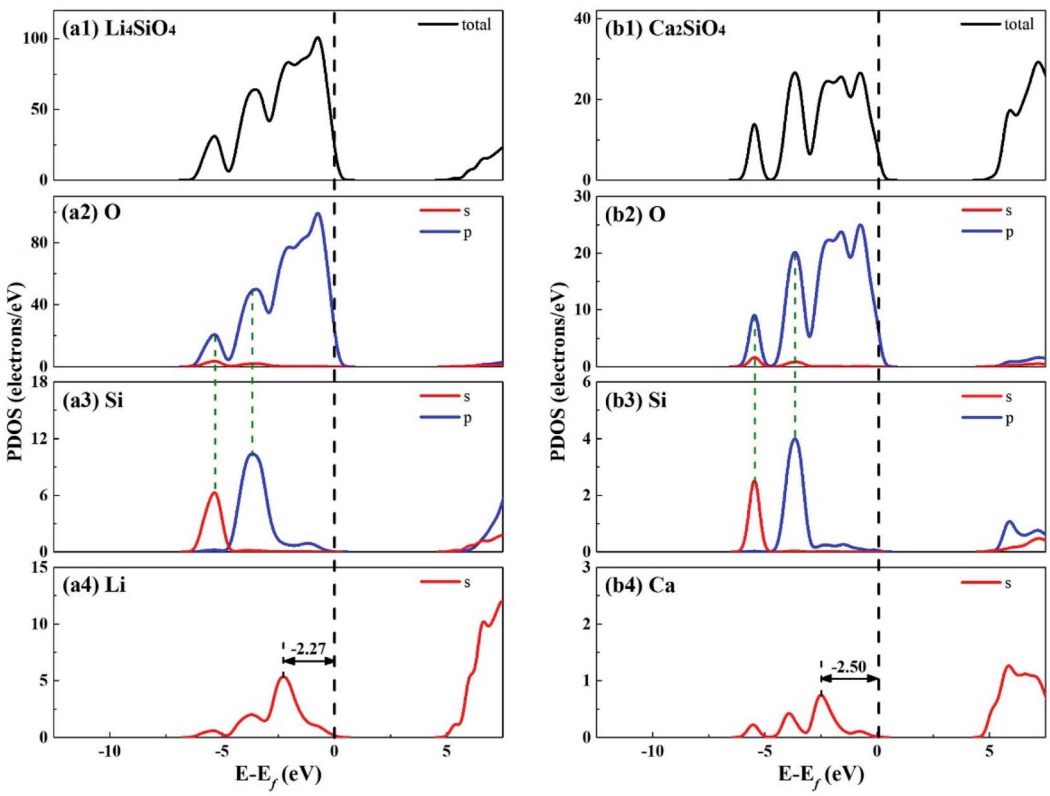

Fig. 3 DOS analysis for (a) Li_4SiO_4 and (b) Ca_2SiO_4. The black dashed line shows the Fermi level.

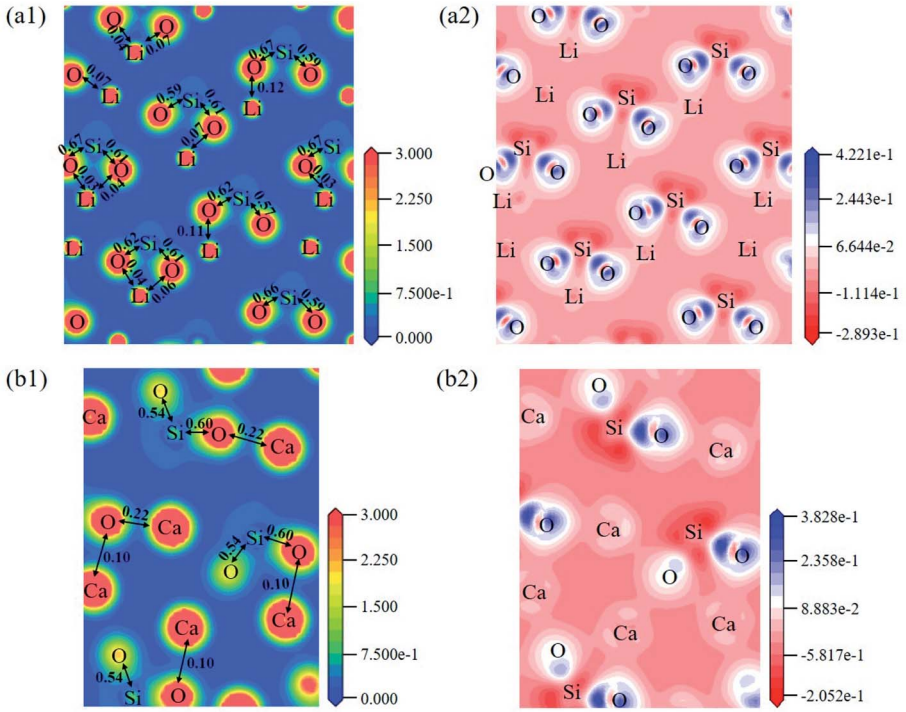

Fig. 4 Contour maps of electron density distributions and differential charge density of (a) Li_4SiO_4 in the plane (010) and (b) Ca_2SiO_4 in the plane (100).

Table 2 The surface energies (E_{surf} in J m^{-2}) of low Miller index surfaces of Li_4SiO_4 and Ca_2SiO_4

Surface	(100)	(010)	(001)	(110)	(101)	(011)	(111)
Li_4SiO_4	1.28	0.78	1.34	0.80	1.28	0.87	0.84
Ca_2SiO_4	0.63	1.19	0.80	0.86	0.66	0.75	0.82

orbitals below and near the E_f. For Li_4SiO_4 and Ca_2SiO_4, their TDOS near the E_f is mainly contributed by the p orbitals of O atoms, suggesting that O atoms are more active and more likely serve as the electron donors. Their PDOS in the region between $-6.55 \sim -2.92$ eV and $-6.25 \sim -3.02$ eV are overlapped with the Si s and p bands, implying orbital hybridization and Si–O binding in the bulks of Li_4SiO_4 and Ca_2SiO_4. However, the states in the region between -3 and 0 eV, near to E_f is about 73% of the total PDOS for O p orbitals for Li_4SiO_4, while that for Ca_2SiO_4 is about 70%. It can be deduced that there are more electronic states for O p orbitals below and near to E_f in Li_4SiO_4 than those in Ca_2SiO_4, Then the electron transfer from O atoms occurs more easier in Li_4SiO_4 than in Ca_2SiO_4.

Furthermore, the first high peak position[41] in the PDOS for Li s orbital of Li_4SiO_4, is closer to the E_f compared with that for Ca s orbital of Ca_2SiO_4, implying that the outer electron of Li

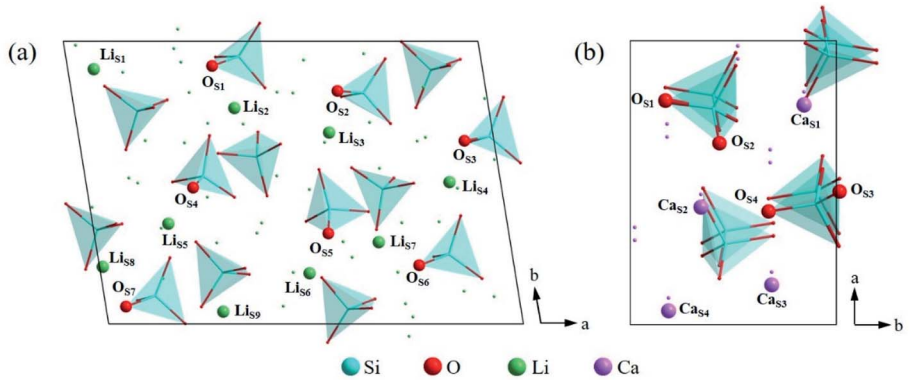

Fig. 5 Atomic arrangement of (a) Li_4SiO_4 (010) surface and (b) Ca_2SiO_4 (100) surface from the top view. The lines and dots represent the underlying atoms and tetrahedra respectively.

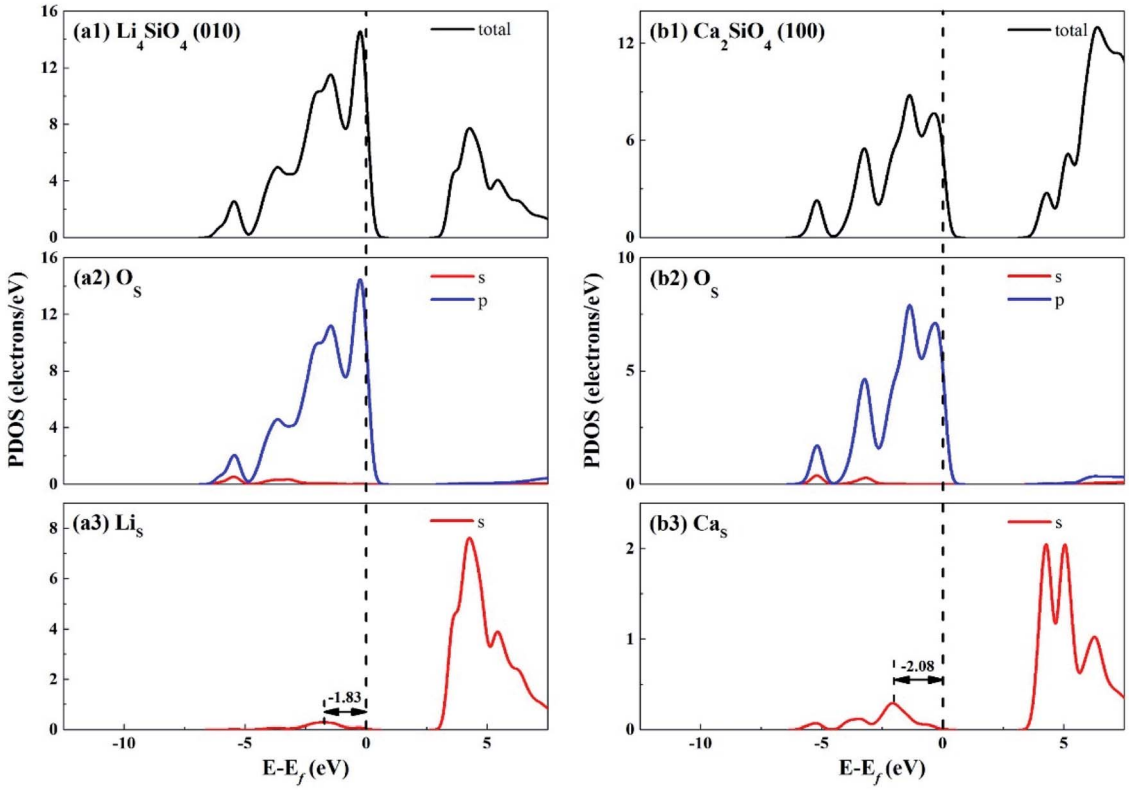

Fig. 6 DOS analysis of the topmost surface layers of (a) Li_4SiO_4 (010) surface and (b) Ca_2SiO_4 (100) surface without CO_2 adsorption. The black dashed line shows the Fermi level.

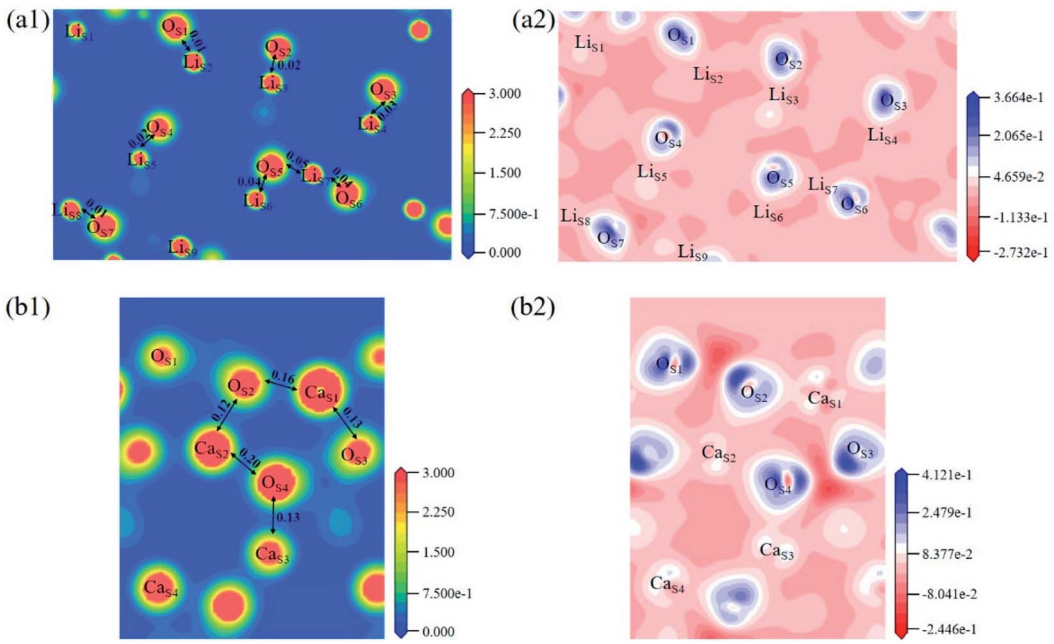

Fig. 7 Contour maps of electron density distributions and differential charge density in the cross sections perpendicular to the (001) plane in (a) Li_4SiO_4 (010) surface and (b) Ca_2SiO_4 (100) surface.

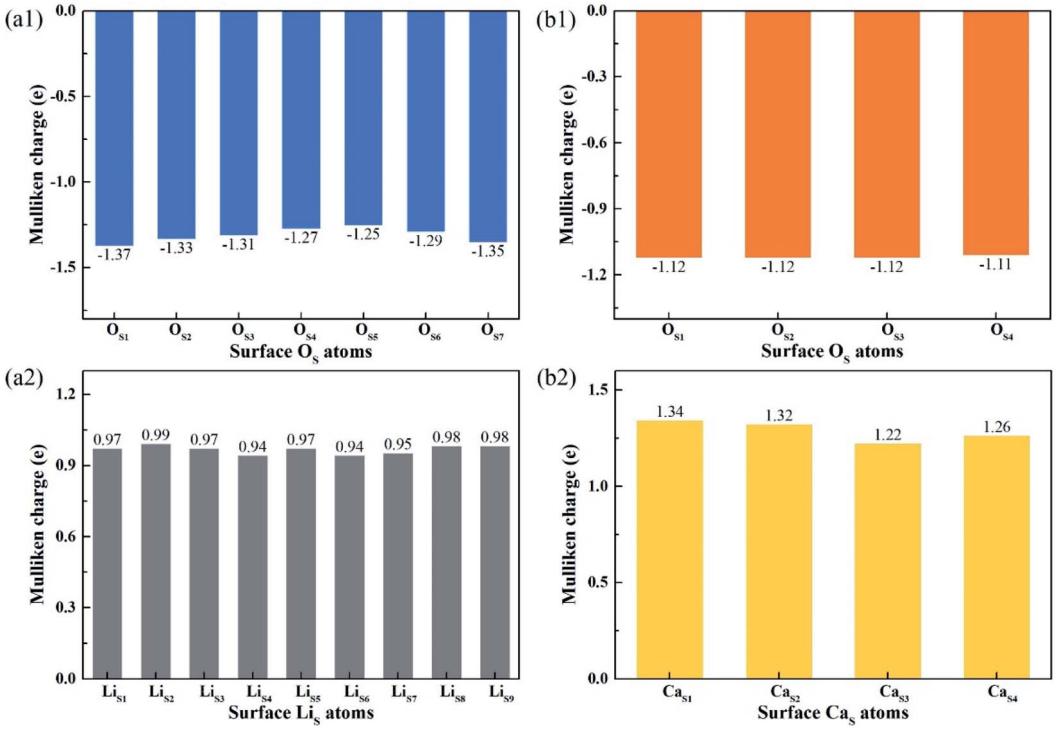

Fig. 8 Mulliken charge analysis of atoms on the topmost surface layers of (a) Li_4SiO_4 (010) surface and (b) Ca_2SiO_4 (100) surface.

atoms in Li_4SiO_4 can be transferred away easier than Ca atoms in Ca_2SiO_4.

The electron density distribution can show the bonding between atoms and differential charge density can show the accumulation and depletion of electrons. In Fig. 4a, electron density between Si and O atoms is higher than surrounding and electrons accumulate in the middle of Si and O atoms, demonstrating that a covalent interaction of Si–O. And according to the charge population marked in the figure, the Si–O covalent interaction is stronger in Li_4SiO_4. Li/Ca–O have a certain covalent interaction and the strength of interaction of Li–O is weaker than Ca–O.

3.2. Structural and electronic properties of surfaces

In order to find out the most stable surface, the surface energies of seven low Miller index surfaces were calculated. The surface energy (E_{surf}) can be calculated according to the eqn (1):[42,43]

$$E_{surf} = (E_{slab} - nE_{bulk})/2A \quad (1)$$

where E_{slab} and E_{bulk} are the total energy of relaxed slab model and unit cell, respectively. n is the number of formula units contained in the slab. A is the area of the slab. According to the calculation results listed in Table 2, the (010) surface and (100) surface were the most stable surface of Li_4SiO_4 and Ca_2SiO_4 respectively, due to their lowest values of surface energy, which is consistent with the previous calculations.[21,22,42] Fig. 5 shows the atomic arrangement of these two surfaces from the top view. The topmost surface layer consists of Li and O atoms for Li_4SiO_4, and Ca and O atoms for Ca_2SiO_4. The atoms of Li, Ca, and O on the topmost surface layer are referred to as Li_S, Ca_S and O_S hereafter, respectively.

The electronic properties of the surfaces should differ from those of the bulks due to the dangling bonds or surface reconstruction. The electronic properties of Li_4SiO_4 (010) surface and Ca_2SiO_4 (100) surface were calculated as well. Fig. 6 shows the TDOS and PDOS of the topmost surface layers of Li_4SiO_4 (010) surface and Ca_2SiO_4 (100) surface. Although the surface TDOS resemble the bulk TDOS shown in Fig. 3 for both Li_4SiO_4 and Ca_2SiO_4, the states of O_S p orbitals are shifted up in energy, and the states in the region between −3 and 0 eV are about 79% of the total PDOS for O_S p orbitals for Li_4SiO_4 (010) surface, while that for Ca_2SiO_4 (100) surface is about 77%. Furthermore, p-band center of O_S atoms increased to −1.725 eV from −1.936 eV of O atoms in bulk Li_4SiO_4, and −1.939 eV from −2.103 eV in bulk Ca_2SiO_4. It can be deduced that the reactivity of the surface O_S atoms is enhanced compared with the O atoms in the bulks. Considering the states near to E_f and the p-band center levels, the O_S atoms in Li_4SiO_4 (010) surface are more prone to suffer the electrophilic attacks with respect to Ca_2SiO_4 (100) surface.

The electron density and differential charge density of the topmost surface layer atoms are shown in Fig. 7. The covalent interaction between Li_S and O_S atoms is weaker than that in bulk, which can be seen from the charge population. While the covalent interaction between Ca_S and O_S atoms is stronger than that in bulk.

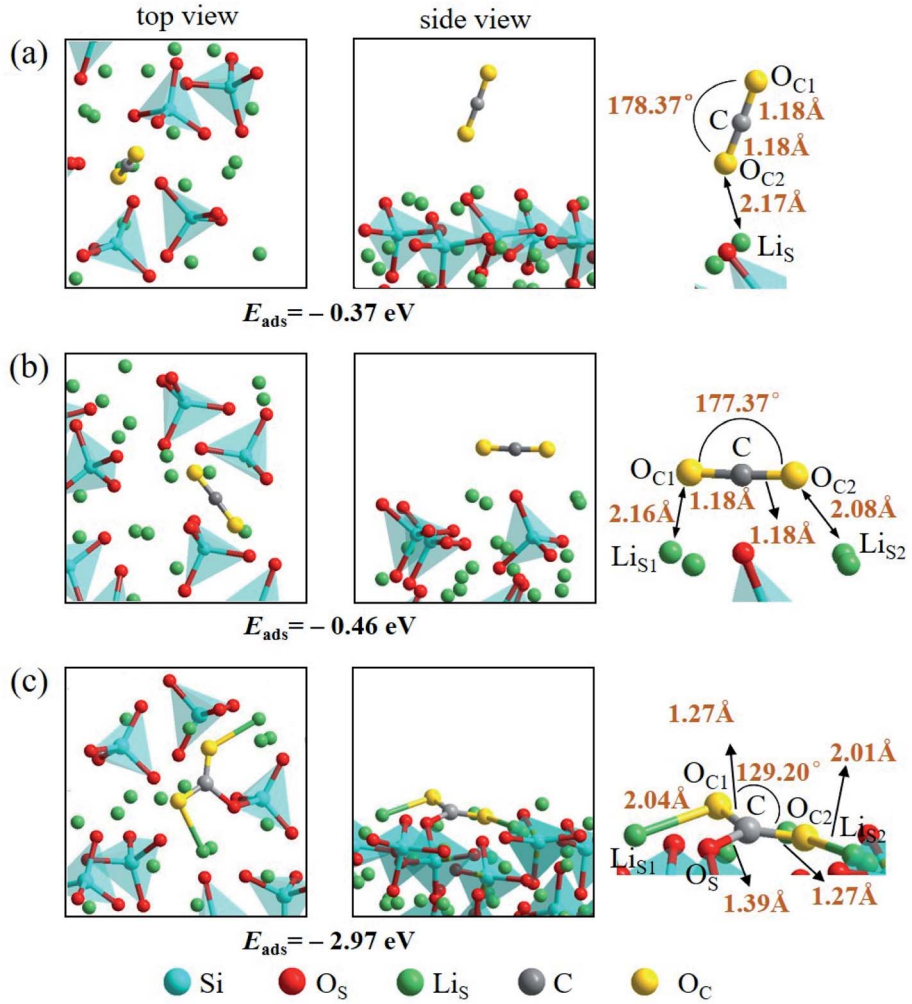

Fig. 9 Three configurations of an adsorbed CO_2 molecule on the Li_4SiO_4 (010) surface: (a) along the normal to the surface, (b) parallel to the surface, (c) bent configuration.

Fig. 8 shows the Mulliken charge of atoms on the topmost surface layer. There is a considerable difference of the charge between bulk atoms (listed in ESI†) and atoms on the topmost surface layer. The positive charge of surface Li_S and Ca_S atoms increases, and the negative charge of the O_S atoms increases compared with bulk atoms. And the deviation of Mulliken charge of surface Li_S atoms from the bulk atoms is relatively large, whereas the Mulliken charge of surface Ca_S and O_S atoms differ from their bulk atoms slightly. Furthermore, the O_S of Li_4SiO_4 (010) surface carry more negative charge than Ca_2SiO_4 (100) surface. According Lewis acid/base theory, O_S atoms of Li_4SiO_4 (010) surface are more basic and easier to lose electrons.

3.3. CO_2 adsorption on the surfaces

The adsorption energy (E_{ads}) of a CO_2 molecule on Li_4SiO_4 (010) surface and Ca_2SiO_4 (100) surface is calculated according to the eqn (2):

$$E_{ads} = E_{slab+CO_2} - (E_{slab} + E_{CO_2}) \quad (2)$$

where $E_{slab+CO_2}$ is the total energy of the surface with CO_2 adsorption, E_{CO_2} is the total energy of an isolated CO_2 molecule. The lower adsorption energy describes the stronger binding between the adsorbed CO_2 molecule and the surface, which reflects the stability of adsorption.

An isolated CO_2 molecule has linear configuration with the length of C–O bond of 1.18 Å. Three adsorption configurations are presented in this study when a CO_2 molecule is adsorbed on the Li_4SiO_4 (010) surface as shown in Fig. 9. In the first configuration, the adsorbed CO_2 molecule almost remains linear configuration along the normal to the Li_4SiO_4 (010) surface. The distance between O atom in CO_2 and the nearest Li_S atom is 2.17 Å, and adsorption energy is −0.37 eV. In the second configuration shown in Fig. 9b, the adsorbed CO_2 molecule has a linear configuration parallel to the Li_4SiO_4 (010) surface, and the adsorption energy is −0.46 eV. In the third configuration shown in Fig. 9c, the adsorbed CO_2 molecule is lying flat on the surface with the bent configuration. The C atom in CO_2 forms a bond with a surface O_S atom with the O_S–C distance of 1.39 Å, and its two oxygen atoms (O_C) are

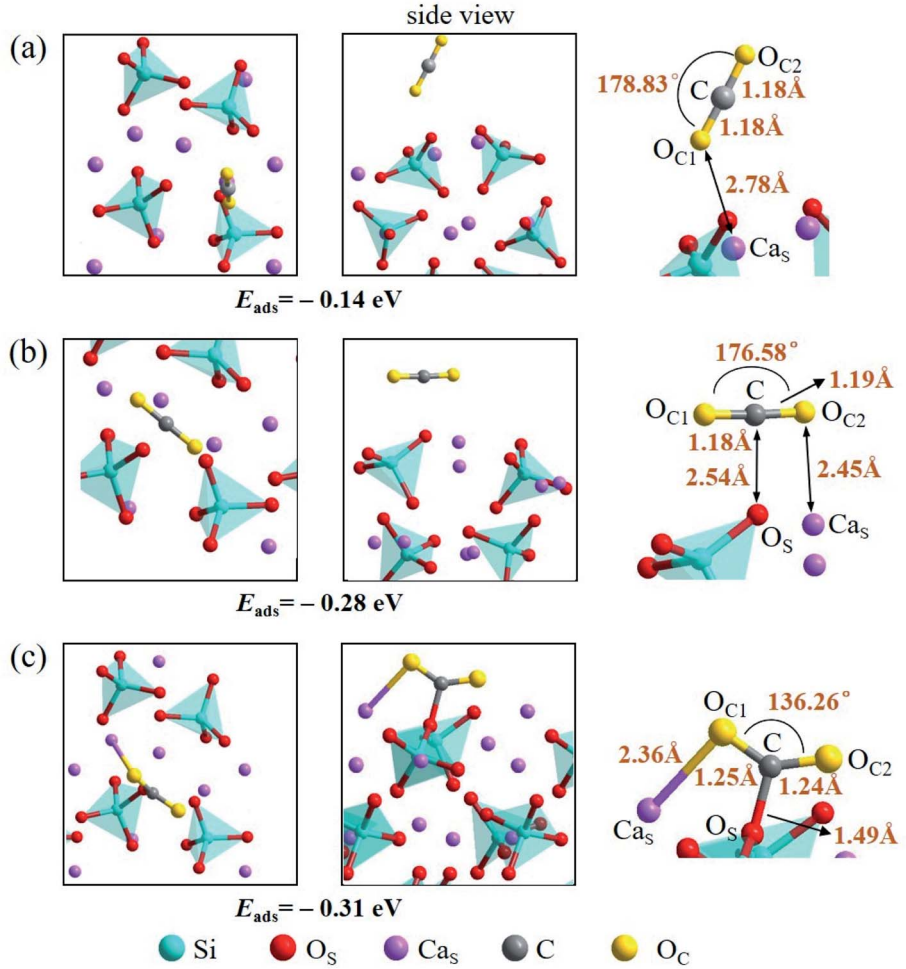

Fig. 10 Three configurations of an adsorbed CO_2 molecule on the Ca_2SiO_4 (100) surface: (a) along the normal to the surface, (b) parallel to the surface, (c) bent configuration.

coordinated to the two surface Li_S atoms, with the O_{C_1}–Li_{S_1} and O_{C_2}–Li_{S_2} distances are 2.04 and 2.01 Å, respectively. The adsorbed CO_2 molecule is bent with an O_{C_1}–C–O_{C_2} angle of 129.20° and the C–O_C length of 1.27 Å. The adsorption energy is −2.97 eV. The third bent configuration of the adsorbed CO_2 on the Li_4SiO_4 (010) surface is energetically favorable over the other two configurations.

There are also three adsorption configurations considered for an adsorbed CO_2 molecule on the Ca_2SiO_4 (100) surface, as shown in Fig. 10. The first configuration, where an almost linearly CO_2 is adsorbed, is in vertical orientation and tilted slightly to the Ca_2SiO_4 (100) surface, and the adsorption energy is −0.14 eV. The absorbed CO_2 molecule is bent a little bit in the second configuration, which is in parallel orientation, and the adsorption energy is −0.28 eV. When the absorbed CO_2 molecule lying on the Ca_2SiO_4 (100) surface in a bent configuration shown in Fig. 10c, the distance of C–O_S is 1.49 Å, and O_{C_1}–C–O_{C_2} angle is 136.26°. The bent configuration has the lowest value of adsorption energy, −0.31 eV in the third configurations.

It is found that the bent configuration consisting of a CO_2 molecule absorbed parallel along to the surface is the most thermodynamically stable among the three configurations considered here for both Li_4SiO_4 and Ca_2SiO_4 surfaces. Furthermore, the Li_4SiO_4 (010) surface has greater adsorption to CO_2 than the Ca_2SiO_4 (100) surface due to the stronger bond between C atom in CO_2 and the surface O_S atom for Li_4SiO_4.

3.4. Partial density of state analysis

Considering that the adsorption energy of adsorbed CO_2 in bent configuration is the lowest, the PDOS calculations were only performed for this configuration, as shown in Fig. 11 and 12. It can be seen that the s and p orbitals of C and O_C of adsorbed CO_2 molecule both move towards lower energy level and broaden compared with the isolated CO_2 molecule, indicating that CO_2 molecule becomes more stable after adsorption. C s and p orbitals of adsorbed CO_2 are hybridized with O_S p orbitals, having bonding character between C and O_S atoms. The states in the region between −3 and 0 eV are about 72% for O_S p orbital for Li_4SiO_4 (010) surface after adsorption, which is

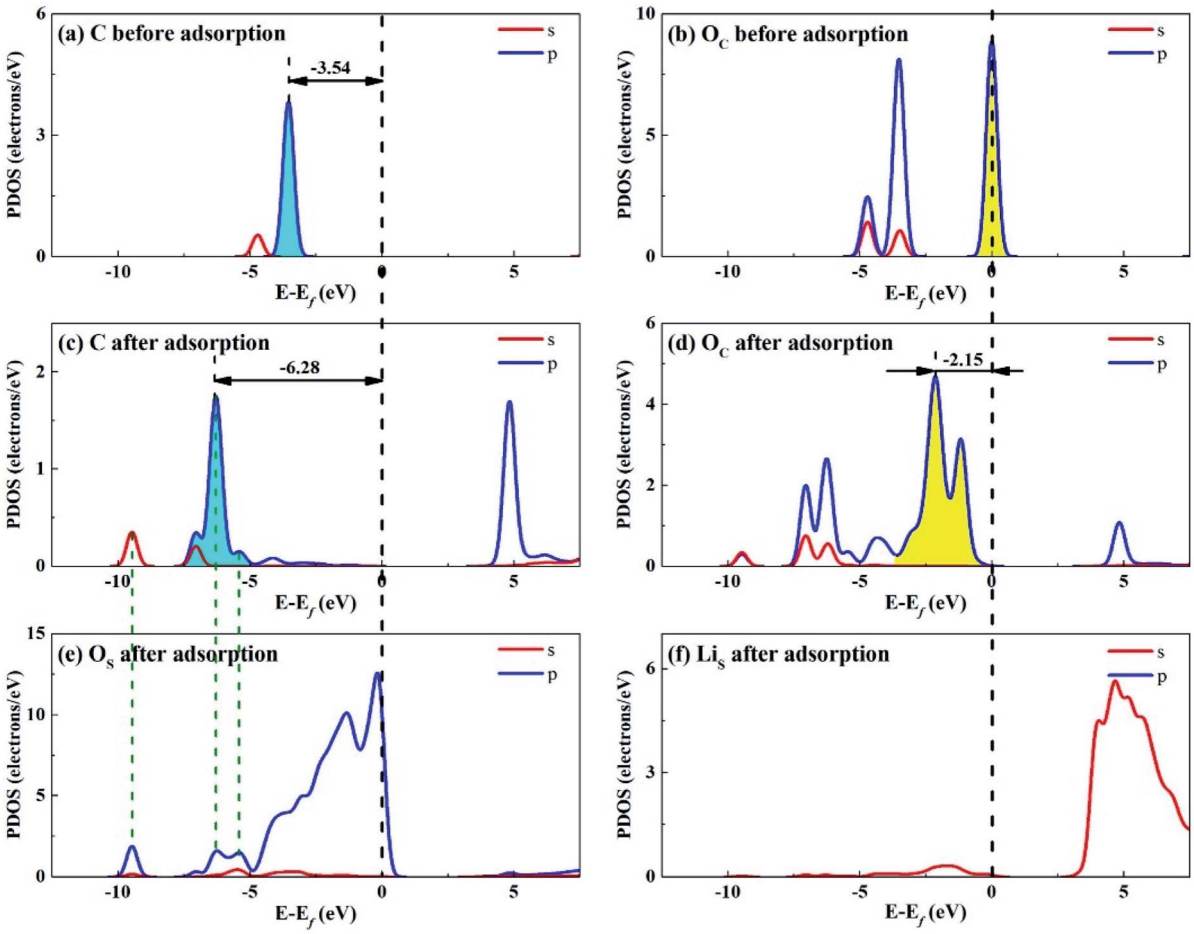

Fig. 11 PDOS analysis of (a) C and (b) O_C atoms of CO_2 before adsorption, (c) C and (d) O_C atoms of CO_2 and (e) O_S and (f) Li_S atoms of Li_4SiO_4 (010) surface after adsorption.

decreased from 79% before adsorption, demonstrating that PDOS of O_S p orbitals is moved to lower energy level after CO_2 adsorption. Furthermore, the PDOS peak of Li_S s orbital become weaker and broader after adsorption.

Fig. 12 shows the PDOS for CO_2 and Ca_2SiO_4 (100) surface after adsorption. Similarly, the s and p orbitals of C and O_C of adsorbed CO_2 move towards lower energy and broaden, but not as far as Li_4SiO_4 (010) surface. It can be deduced that CO_2 adsorption on Li_4SiO_4 (010) surface is more stable. The states in the region between −3 and 0 eV are about 73% for O_S p orbitals for Ca_2SiO_4 (100) surface. The PDOS peaks for Ca_S s orbital become weaker and broader after adsorption, similar to Li_S s orbital.

To better elucidate the different CO_2 absorption behaviors of Li_4SiO_4 (010) and Ca_2SiO_4 (100) surfaces, the p-band centers of C and O_C in CO_2 and O_S on the surfaces with and without CO_2 absorption were calculated, and the results were shown in Fig. 13. Comparing the p-band centers of O_S atoms on two clean surfaces, it can be found that the p-band center of O_S atoms on the Li_4SiO_4 (010) surface is closer to the E_f than that of Ca_2SiO_4 (100) surface, which means the O_S atoms of Li_4SiO_4 (010) surface are more active and easier to transfer electrons to CO_2 absorbed. When CO_2 is adsorbed on the Li_4SiO_4 (010) surface, it is obvious that p-band centers of C, O_C and O_S atoms are farther away from the E_f, indicating that CO_2 absorbed and O_S become stable. On the other hand, energy-down shift of the p-band centers of C, O_C and O_S atoms of Ca_2SiO_4 (100) surface due to CO_2 adsorption is much smaller compared with Li_4SiO_4 (010) surface, probably leading to its higher absorption energy and less CO_2 absorption.

3.5. Mulliken charge analysis

To understand the interactions and charge distributions associated with CO_2 adsorbed with the most energetically favorable configurations on Li_4SiO_4 (010) and Ca_2SiO_4 (100) surfaces, a Mulliken charge anlysis was performed. The detail date of Mulliken charges for CO_2 and Li_4SiO_4 (010) and Ca_2SiO_4 (100) surfaces before and after adsorption were shown in Fig. 14. For CO_2 adsorbed on Li_4SiO_4 (010) surface, it is found that the Mulliken charge on a surface O_S atom changes from $-1.33e$ to $-0.86e$, while the charges on the surface Li_{S_1} and Li_{S_2} atoms increase from $0.93e$ to $0.96e$, and from $0.93e$ to $0.95e$, respectively. It can be deduced that CO_2 adsorption induces the net

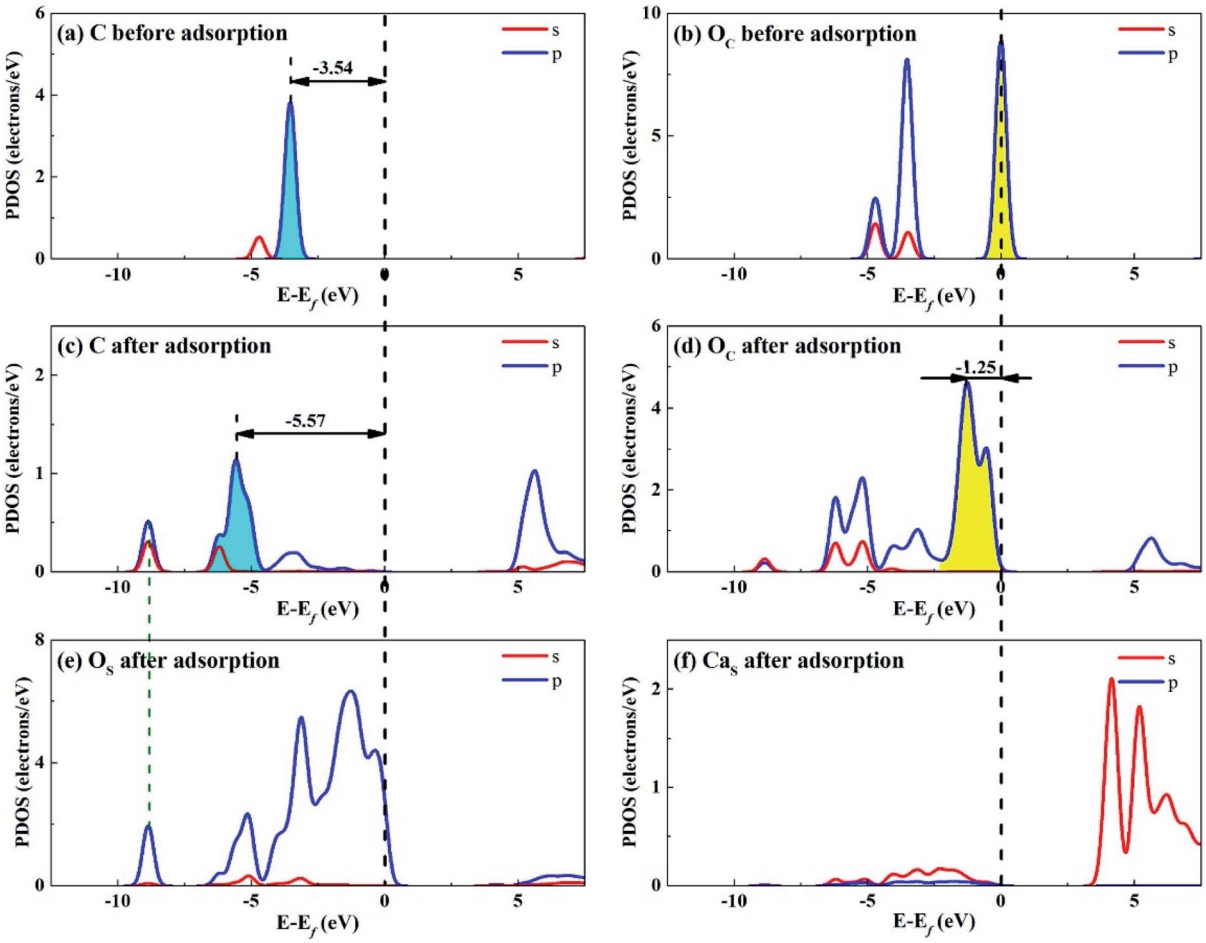

Fig. 12 PDOS analysis of (a) C and (b) O_C atoms of CO_2 before adsorption, (c) C and (d) O_C atoms of CO_2 and (e) O_S and (f) Ca_S atoms of Ca_2SiO_4 (100) surface after adsorption.

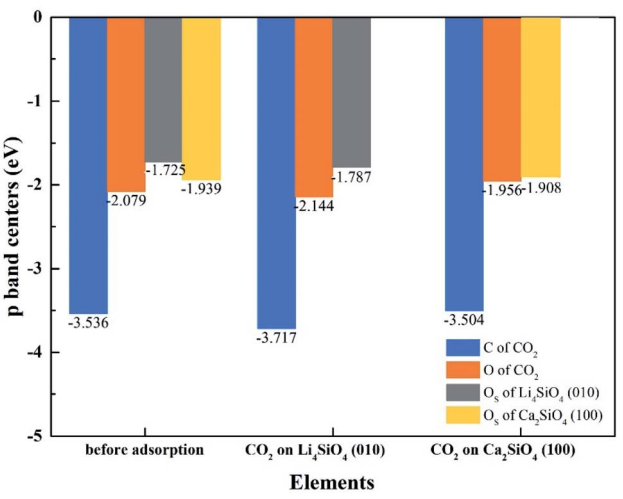

Fig. 13 The p-band centers of C 2p and O 2p orbitals of CO_2, Li_4SiO_4 (010) surface and Ca_2SiO_4 (100) surface before and after adsorption.

electron loss of Li_4SiO_4 (010) surface. On the other side, the Mulliken charge of C atom in CO_2 adsorbed decreases from 0.98*e* to 0.76*e*, and the charges of O_{C_1} and O_{C_2} from −0.49*e* to −0.78*e* and −0.76*e*, respectively, which means that CO_2 adsorbed gains the charges from Li_4SiO_4 (010) surface.

In the case of CO_2 adsorption on Ca_2SiO_4 (100) surface, it is found that charge gain for C atom in CO_2 adsorbed is similar to that on Li_4SiO_4 (010) surface, but charges gained by O_{C1} and O_{C2} atoms are fewer. Furthermore, the Mulliken charge on an O_S atom on Ca_2SiO_4 (100) surface changes from −1.12*e* to −0.88*e*, and the charge on the surface Ca_S from 1.34*e* to 1.40*e*. The net charge transfer from Ca_2SiO_4 (100) surface to CO_2 adsorbed is much less compared to that Li_4SiO_4 (010) surface.

The charge population between C in CO_2 adsorbed and a surface O_S atom was calculated to be 0.62 and 0.45 for Li_4SiO_4 (010) and Ca_2SiO_4 (100) surfaces, respectively. It can be deduced that the C–O_S covalent interaction on Li_4SiO_4 (010) surface is even stronger, which leads to the stronger adsorption of CO_2.

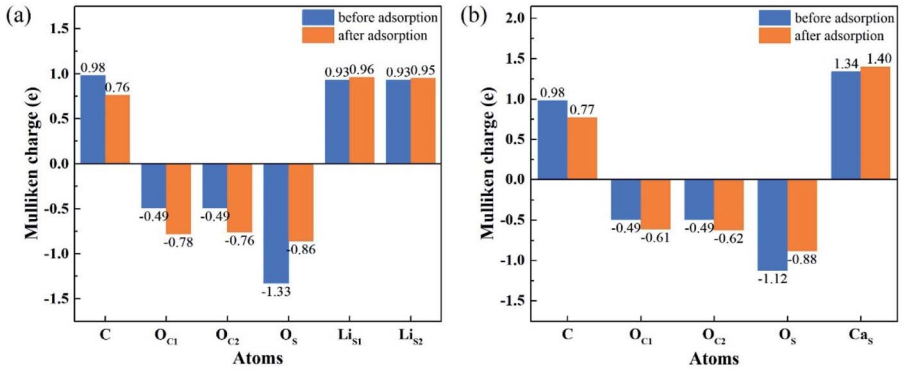

Fig. 14 Mulliken charge analysis of adsorbed CO_2 molecule and (a) Li_4SiO_4 (010) surface, and (b) Ca_2SiO_4 (100) surface before and after adsorption.

4. Conclusions

A density functional theory calculation was conducted to research the CO_2 adsorption on the Li_4SiO_4 (010) and Ca_2SiO_4 (100) surfaces. The bent configuration consisting of a CO_2 molecule adsorbed parallel along to the surface is the most thermodynamically favorable for Li_4SiO_4 and Ca_2SiO_4 surfaces. And the adsorption energy of Li_4SiO_4 (010) surface is −2.97 eV, more negative than Ca_2SiO_4 (100) surface, −0.31 eV. Li_4SiO_4 (010) surface is more favorable for forming a stronger covalent bond between a surface O_S atom to the C atom of CO_2 adsorbed and transferring more charges to adsorbed CO_2. In addition, it was found that the Mulliken charge of O_S atoms on the Li_4SiO_4 (010) is more negative, and its p-band center is closer to the E_f, which implies O_S atoms of Li_4SiO_4 (010) are more active and more likely serve as the electron donors with respect to Ca_2SiO_4 (100) surface.

Conflicts of interest

There are no conflicts to declare.

Acknowledgements

This work was financially supported by the Natural Science Foundation of China (No. 51574163).

References

1 R. Ben-Mansour, M. A. Habib, O. E. Bamidele, M. Basha, N. A. A. Qasem, A. Peedikakkal, T. Laoui and M. Ali, *Appl. Energy*, 2016, **161**, 225.
2 M. Seggiani, M. Puccini and S. Vitolo, *Int. J. Greenhouse Gas Control*, 2013, **17**, 25.
3 M. Kato, S. Yoshikawa and K. Nakagawa, *J. Mater. Sci. Lett.*, 2002, **21**, 485.
4 M. Kato, K. Nakagawa, K. Essaki, Y. Maezawa, S. Takeda, R. Kogo and Y. Hagiwara, *Int. J. Appl. Ceram. Technol.*, 2005, **2**, 467.
5 K. Wang, Z. Yin and P. Zhao, *Ceram. Int.*, 2016, **42**, 2990.
6 M. E. Bretado, V. G. Velderrain, D. L. Gutiérrez, V. Collins-Martínez and A. L. Ortiz, *Catal. Today*, 2005, **107–108**, 863.
7 K. Essaki and M. Kato, *J. Mater. Sci.*, 2005, **4**, 1.
8 R. Rodríguez-Mosqueda and H. Pfeiffer, *J. Phys. Chem.*, 2010, **114**, 4535.
9 M. J. Venegas, E. Fregoso-Israel, R. Escamilla and H. Pfeiffer, *Ind. Eng. Chem. Res.*, 2007, **46**, 2407.
10 S. Jeoung, J. H. Lee, H. Y. Kim and H. R. Moon, *Thermochim. Acta*, 2016, **637**, 31.
11 I. C. Romero-Ibarra, J. Ortiz-Landeros and H. Pfeiffer, *Thermochim. Acta*, 2013, **567**, 118.
12 V. L. Mejía-Trejo, E. Fregoso-Israel and H. Pfeiffer, *Chem. Mater.*, 2008, **20**, 7171.
13 G. V. Tomarov, Y. V. Petrov, A. A. Shipkov, O. A. Dovgii, V. N. Semenov and A. V. Mikhailov, *Therm. Eng.*, 2008, **55**, 154.
14 M. Zhao, J. Shi, X. Zhong, S. Tian, J. Blamey, J. Jiang and P. S. Fennell, *Energy Environ. Sci.*, 2014, **7**, 3291.
15 M. Zhao, Y. Song, G. Ji and X. Zhao, *Energy Fuels*, 2018, **32**, 5443.
16 Y. S. Kim and S. G. Kang, *Appl. Surf. Sci.*, 2019, **486**, 571.
17 A. Kumar, F. Ropital, T. de Bruin and B. Diawara, *Appl. Surf. Sci.*, 2020, **529**, 147127.
18 S. G. Kang, *J. CO_2 Util.*, 2020, **42**, 101293.
19 Y. Duan and K. Parlinski, *Phys. Rev. B: Condens. Matter Mater. Phys.*, 2011, **84**, 104113.
20 T. Tang, P. Chen, W. Luo, D. Luo and Y. Wang, *J. Nucl. Mater.*, 2012, **420**, 31.
21 X. Kong, Y. Yu, S. Ma, T. Gao, C. Xiao and X. Chen, *Chem. Phys. Lett.*, 2018, **691**, 1.
22 C. Qi, D. Spagnoli and A. Fourie, *Appl. Surf. Sci.*, 2020, **518**, 146255.
23 Q. Wang, H. Manzano, I. López-Arbeloa and X. Shen, *Minerals*, 2018, **8**, 1.
24 Q. Wang, F. Li, X. Shen, W. Shi, X. Li, Y. Guo, S. Xiong and Q. Zhu, *Cem. Concr. Res.*, 2014, **57**, 28.
25 M. C. Payne, M. P. Teter, D. C. Allan, T. A. Arias and J. D. Joannopoulos, *Rev. Mod. Phys.*, 1992, **64**, 1045.
26 J. P. Perdew, K. Burke and M. Ernzerhof, *Phys. Rev. Lett.*, 1996, **77**, 3865.

27 B. Hammer, *Phys. Rev. B: Condens. Matter Mater. Phys.*, 1999, **59**, 7413.
28 J. P. P. Ramalho, J. R. B. Gomes and F. Illas, *RSC Adv.*, 2013, **3**, 13085.
29 S. Grimme, J. Antony, S. Ehrlich and H. Krieg, *J. Chem. Phys.*, 2010, **132**, 154104.
30 D. J. Chadi, *Phys. Rev. B*, 1977, **16**, 1746.
31 B. G. Pfrommer, M. Côté, S. G. Louie and M. L. Cohen, *J. Comput. Phys.*, 1997, **131**, 233.
32 A. Belsky, M. Hellenbrandt, V. L. Karena and P. Lukschb, *Acta Crystallogr.*, 2002, **58**, 364.
33 R. Zhang, S. Ma, Q. Wang, C. Xiao, C. Zhang and T. Gao, *Ceram. Int.*, 2020, **46**, 8192.
34 Q. Guan, T. Gao, Y. Shen, S. Ma, T. Lu, X. Chen, C. Xiao and X. Long, *Int. J. Mod. Phys. B*, 2015, **29**, 1550128.
35 D. Tranqui, R. D. Shannont and H. Y. Chen, *Acta Crystallogr. B*, 1979, **35**, 2479.
36 C. Haitao, H. Xuefei and H. Weigang, *Rare Met. Mater. Eng.*, 2018, **47**, 729.
37 C.-J. Chan, W. M. Kriven and J. F. Young, *J. Am. Ceram. Soc.*, 1988, **71**, 713.
38 Y. J. Kim, I. Nettleship and W. M. Kriven, *J. Am. Ceram. Soc.*, 1992, **75**, 2407.
39 A. V. Marenich, S. V. Jerome, C. J. Cramer and D. G. Truhlar, *J. Chem. Theory Comput.*, 2012, **8**, 527.
40 K. H. Jost, B. Ziemer and R. Seydel, *Acta Crystallogr.*, 1977, **33**, 1696.
41 W. Tao, C. Zhu, Q. Xu, S. Li, X. Xiong, H. Cheng, X. Zou and X. Lu, *ACS Omega*, 2020, **5**, 20090.
42 E. Durgun, H. Manzano, P. V. Kumar and J. C. Grossman, *J. Phys. Chem. C*, 2014, **118**, 15214.
43 W.-B. Zhang, C. Chen and S.-Y. Zhang, *J. Phys. Chem. C*, 2013, **117**, 21274.